Analytical Method with Iteration Technique (AMIT) and Finite Element Method (FEM) for Predicting the Flexural Performance of Glulam Wood/PVC Composite Hollow Member

Phatthana Aunyingcharoen,[a] Tawich Pulngern,[b,*] Vichai Rosarpitak,[c] and Narongrit Sombatsompop [d]

*Corresponding author: Tawich.pul@kmutt.ac.th

DOI: 10.15376/biores.19.3.5197-5226

GRAPHICAL ABSTRACT

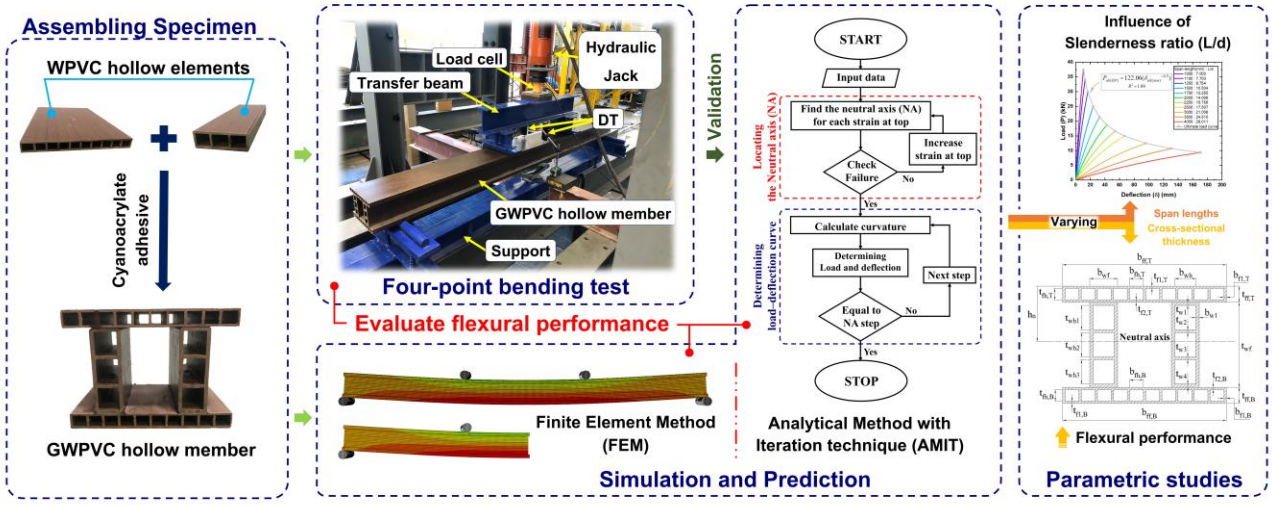

Analytical Method with Iteration Technique (AMIT) and Finite Element Method (FEM) for Predicting the Flexural Performance of Glulam Wood/PVC Composite Hollow Member

Phatthana Aunyingcharoen,[a] Tawich Pulngern,[b,*] Vichai Rosarpitak,[c] and Narongrit Sombatsompop [d]

The flexural performance of a glulam wood/PVC composite (GWPVC) hollow member, which was assembled from four elements with WPVC composite hollow sections to create a double I-section, was studied using two methods: the analytical method with iteration technique (AMIT) and the finite element method (FEM). Experiments verified the predictions from AMIT and simulations from FEM to determine the most suitable method for the parametric studies. This investigation explored the variations in slenderness ratio and the flange and web thickness to enhance and study their impact on flexural performance. In parametric studies, equal cross-sectional areas were used to facilitate comparisons and maintain production costs. The importance of bond strength at the contact surfaces in assembling a GWPVC hollow member led to bonding tests and confirmed sufficient strength at contact surfaces. In four-point bending tests, the GWPVC hollow member exhibited a brittle mode with flexural tensile failure without delamination. The initial MOE, MOR, and maximum deflection values were 5,140 MPa, 29.8 MPa, and 47.8 mm, respectively. The parametric study employs AMIT to investigate flexural performance and reveals that varying the slenderness ratio affected the initial stiffness, maximum deflection, and ultimate load. Flexural performance can be improved by making minor adjustments.

DOI: 10.15376/biores.19.3.5197-5226

Keywords: Analytical method; Ethyl cyanoacrylate; Finite element method; Glulam WPVC composite; Iteration technique; WPVC composite

*Contact information: a: Ph.D. candidate, Department of Civil Engineering, Faculty of Engineering, King Mongkut's University of Technology Thonburi (KMUTT), 126 Pracha-Uthit, Bangmod, Thungkru, Bangkok, 10140, Thailand; b: Associate Professor, Department of Civil Engineering, Faculty of Engineering, King Mongkut's University of Technology Thonburi (KMUTT), 126 Pracha-Uthit, Bangmod, Thungkru, Bangkok, 10140, Thailand; c: V.P. Wood Co., Ltd., 72/1 Moo. 4, Suksawat 41, Banphueng, Phra Pradaeng, Samut Prakan, 10130, Thailand; d: Polymer PROcessing and Flow (P-PROF) Research Group, Materials Technology Programme, School of Energy, Environment and Materials, King Mongkut's University of Technology Thonburi (KMUTT), 126 Pracha-Uthit, Bangmod, Thungkru, Bangkok, 10140, Thailand; *Corresponding author: Tawich.pul@kmutt.ac.th*

INTRODUCTION

Timber is a natural material that is widely used due to its aesthetic appeal and impressive strength. It is used in various applications, including buildings, decorations, and furniture. Different processing techniques, such as cutting, sanding, chemical treatment, or thermal modification (Pulngern *et al.* 2020), are employed to enhance its usability.

In Thailand, the growing demand for timber in structural and decorative applications has resulted in rising prices, a shortage of trees, and a continual reduction in their numbers. Therefore, conserving the remaining trees is necessary. One alternative to timber is a wood-plastic composite (WPC). Such composites offer advantages, such as a wood-like appearance, lightweight nature, resistance to swelling, non-flammability, low maintenance requirements, and protection against moisture and termite damage (Chetanachan *et al.* 2001). WPC primarily consists of plastic and wood sawdust; thus, producing WPC increases the value of wood sawdust by recycling it as a raw material instead of incinerating it. Furthermore, several types of plastic can be used in WPC production (Jian *et al.* 2022). Recycled plastics have been investigated for their potential as WPC matrix materials (Bhaskar *et al.* 2012; Luo and Cheng 2021). Therefore, the use of WPC may increase due to the current growing trend of environmental conservation.

Typically, WPC is produced using polyethylene (PE) or polypropylene (PP); both are polyolefins. While polyolefins remain widely used as matrix materials, the superior mechanical properties of polyvinyl chloride (PVC) make it an outstanding option for the matrix of WPC. The confirmation of these mechanical properties is supported by previous research on WPC made from PVC (WPVC composite). This research has revealed higher tensile, compressive, and flexural strength in WPVC composites compared to WPC produced from PE and PP (Tunsakul 2006). However, another study has found that differences in the type or quantity of wood sawdust and additives may influence outcomes (Ratanawilai and Taneerat 2018). Therefore, using PVC as the matrix material offers improved durability and enhanced strength, making it a popular choice for producing WPC in Thailand. Moreover, WPVC composites are commonly used in applications such as Anderson windows. As a result, WPVC composite has become a material of interest.

PVC is a plastic that is different from other types of plastic due to its polar nature, which, in principle, makes it compatible with the surface of wood. Because hydrogen bonds are formed between the polar nature of PVC and the hydroxyl groups of wood, this enhances the adhesion between PVC and wood particles. However, these hydrogen bonds can be broken if they contain moisture. The formation of new hydrogen bonds with water results in reduced adhesion between the wood and the PVC, causing a reduction in mechanical properties (Sombatsompop and Chaochanchaikul 2004). Additionally, the wood particles are treated with a coupling agent (aminosilane) before producing the WPVC composite to increase the adhesion between wood fiber and PVC, resulting in higher mechanical properties (Sombatsompop *et al.* 2003). The adhesion increases because the coupling agent changes the surface of the wood fiber from hydrophilic to hydrophobic, causing the surface tension of the wood to decrease, which improves wetting, diffusion of the polymer into the surface of wood fibers, and mechanical interlocking. This results in increased adhesion (Shah *et al.* 2005; Prachayawarakorn *et al.* 2008).

The properties of WPVC composite are heterogeneous; they are likely anisotropic (Sombatsompop *et al.* 2010). The composite has demonstrated lower mechanical properties than timber (Chetanachan *et al.* 2001; Pulngern *et al.* 2011). Several studies have aimed to enhance its mechanical properties by adjusting the composition, for example, increasing the amount of untreated sawdust in a WPVC composite mixture. However, when its quantity in the mixture reached a certain point, the mechanical properties decreased at a slower rate (Sombatsompop *et al.* 2003). In contrast, using chemically surface-treated wood sawdust in an appropriate quantity has been shown to improve mechanical properties (Jeamtrakull *et al.* 2012). Additionally, recent research has found that using a higher proportion of rubberwood sawdust compared to teak sawdust in the WPVC composite

mixture resulted in better mechanical properties (Kanking *et al.* 2023). Furthermore, incorporating compatibilizers improved the compatibility between the wood sawdust and the plastic, enhancing tensile properties (Sombatsompop and Chaochanchaikul 2005). Moreover, integrating various types of fibers into the mixture of WPVC composites has been shown to enhance their mechanical properties (Chen *et al.* 2017).

For the production process of WPVC composite, the production temperature is between 140 and 170 °C (Kanking *et al.* 2021), which is considered a high temperature. Therefore, the risk of wood particles scorching should be considered. Due to the decomposition temperature (T_d) of the WPVC composite being approximately 235 °C (Sombatsompop *et al.* 2008) and the glass transition temperature (T_g) of the PVC being in the range of 80 to 100 °C (Prachayawarakorn *et al.* 2005), the temperature used in the production process was higher than T_g but lower than T_d. This results in the PVC being molten without decomposing and encapsulating the wood particles, which prevents the wood particles from being directly exposed to excessively high temperature used in production, resulting in no scorching. In addition, additives such as PVC emulsion, thermal stabilizer, and lubricants (Kanking *et al.* 2021) are used to prevent PVC from decomposing and ensure smooth flow during the production process.

External factors significantly influence the properties of WPVC composites in practical applications. For instance, the WPVC composite has better flexural and tensile properties in the direction of extrusion than in the direction perpendicular to the extrusion (Roman *et al.* 2018). Moisture levels vary inversely with their mechanical properties (Sombatsompop *et al.* 2004). Exposure to UV weathering affects the thermal degradation of PVC and the color fading of the wood in WPVC composites. However, incorporating Tinuvin P, a UV stabilizer, improved the color stability of WPVC composites under UV weathering conditions (Chaochanchaikul *et al.* 2013). Furthermore, several research studies have attempted to enhance the resistance of WPVC composites to degradation using approaches such as coating them with CeO_2-based acrylic, a UV absorber, as a surface layer. This process enhanced UV resistance while maintaining hydrophilicity levels and mechanical properties under UV weathering conditions (Pattamasattayasonthi *et al.* 2011). Additionally, incorporating 3-iodopropinyl-N-butylcarbamate (IPBC), a fungicide, into the WPVC composite composition significantly retarded deterioration from fungal attack (Kositchaiyong *et al.* 2014). These methods effectively maintained the mechanical properties and aesthetics of WPVC composites in practical applications.

Due to the limited size and shape of the WPVC composite hollow element cross-sections currently available in Thailand and their material properties, which are lower than timber, they are primarily used for decorative or non-structural purposes, such as ceilings and facades. Despite attempts to strengthen WPVC composite hollow elements with flat bar strips, their modulus of rupture (MOR) remained moderate. However, it was higher than that of the unstrengthened WPVC composite hollow element (Pulngern *et al.* 2011, 2013). Additionally, research has attempted to enhance the flexural performance of WPC composite beams with an I-section, a cross-section rarely used for this material in Thailand, by using a grooving technique and reinforcing with glass fiber–reinforced polymer (GFRP), resulting in improved flexural performance without delamination (Naghipour *et al.* 2013). Furthermore, increasing the depth of the section is an alternative option to enhance the flexural performance of the member without reinforcement. This approach can enhance flexural performance and reduce the additional processes required for reinforcing the member with other materials. Therefore, expanding the cross-section becomes an interesting choice to enhance flexural performance, which may be improved until it is

sufficient for structural purposes, similar to glulam timber, where this technique has been successfully applied.

The glulam method, which is commonly used to expand the cross-section of timber material, has been extensively studied. In this method, small pieces of wood are typically used, and finger joints are employed to extend the length of the laminated lumber. Subsequently, these laminate lumber pieces are bonded to form glulam timber, resulting in a laminating effect value calculated from the ratio of the flexural strength to the tensile strength within a range between 0.95 and 2.51 (Falk and Colling 1995). This finding aligns with another study, which suggested that the glulam technique can enhance cross-sectional dimensions by bonding small timbers with adhesive while maintaining material properties comparable to an equivalently sized timber (Udtaranakron *et al.* 2023). Furthermore, the glulam process offers unlimited flexibility in shaping and improves overall performance by reducing or eliminating the negative aspects of wood (Mohamad *et al.* 2011; Nadir and Nagarajan 2014; Maricar *et al.* 2022). In addition to using the glulam method for expanding cross-sectional dimensions, previous research using the glulam method has focused on strengthening glulam timber to reduce the amount of top-grade timber on the extreme tension face (Issa and Kmeid 2005) or enhancing flexural performance through strengthening techniques, such as incorporating carbon fiber–reinforced polymer (CFRP), glass fiber–reinforced polymer (GFRP), and steel in various forms (Glišović *et al.* 2016; Nadir *et al.* 2016; İşleyen *et al.* 2021; Yang and Zhang 2021; Peixoto *et al.* 2022; Zamli *et al.* 2022; Ulaşan *et al.* 2023). However, the glulam method of timber preparation may necessitate finger joints, which have been identified as the weak points in glulam timber (Hamid *et al.* 2015). Thus, there have been efforts to strengthen the glulam timber at the finger joints to improve flexural performance (Khelifa *et al.* 2016). Adapting the glulam method to WPVC composite hollow elements may offer many advantages, such as enhanced cross-sectional and improved flexural performance. Furthermore, WPVC composite hollow elements can be manufactured with long spans, eliminating the finger joints that are the weak points in glulam timber.

Prior research has expanded WPVC composite hollow elements using the glulam method, employing adhesive bonding to create a log wall. The present study investigated compressive load, as well as thermal and acoustic properties. Increased web thickness and reduced flange spacing in WPVC log wall cross-sections enhanced ultimate compressive load and reduced noise (Pulngern *et al.* 2017). Similarly, the glulam method has been used to enhance lateral load resistance in large-scale structures of WPVC log walls, and the behavior of first log-foundation connections under in-plane lateral loads, both monotonic and cyclic, has been investigated. The findings revealed differences in the load-resisting behavior of connections despite equal load-bearing areas (Eakintumas *et al.* 2022a). Furthermore, the load-bearing capacity of a WPVC log wall with openings has been investigated using FEM and validating the accuracy of the model by comparing the results with other research that studied timber log walls (Bedon and Fragiacomo 2015). The results revealed that a WPVC log wall with two openings met the ACI318 requirements for a load-bearing wall in a single-story house with a roof span of up to 4 meters (Eakintumas *et al.* 2022b). Moreover, comparing the temperature profiles and energy consumption of WPVC and fiber cement houses under solar exposure revealed that WPVC composite is a better housing insulator than fiber cement board, commonly used for walls (Kanking *et al.* 2021).

WPVC composites have limitations in applications due to moderate mechanical properties and the dimensional constraints of commercially available WPVC composite hollow elements in Thailand. Although recent research has used the glulam method with

WPVC composite hollow elements to overcome dimensional constraints for creating load-bearing walls (Pulngern *et al.* 2017; Eakintumas *et al.* 2022a, 2022b), the application of this method for creating flexural members remains unexplored. This research uses the glulam method to enhance the cross-sectional dimensions of WPVC composite hollow elements to extend their usage as flexural members in building structures, such as floors or beams. The assembly of glulam WPVC composite (GWPVC) hollow members use commercially available WPVC composite hollow elements. The cross-section of the GWPVC hollow member is assembled with adhesive to form a double I-beam section, which has lightweight characteristics and contains channels for sanitary or electrical systems. In this study, the finite element method (FEM) was employed for simulating flexural performance. Furthermore, the analytical method was also used to predict flexural performance and broaden the investigation options for GWPVC hollow members. This method is based on previous research that calculates the position of the neutral axis from the equilibrium of forces in the cross-section and then calculates the curvature to evaluate deflection of the beam (Naghipour *et al.* 2011). However, the analytical method is similar to the generalized nonlinear constitutive law (GNCL), which is used to analyze the bending of beams and plates. The next step was to employ the Finite Element Method to determine deflections and rotations, ultimately leading to the calculation of curvature (Mrówczyński *et al*. 2021a,b; Staszak *et al.* 2021, 2022). Therefore, this research explored flexural performance through four-point bending tests and used both methods, FEM simulations (ABAQUS software) and AMIT predictions (MATLAB), to assess flexural performance.

After assembling a GWPVC hollow member, one of several convenient methods for enhancing flexural performance is adjusting the thickness of the various sections within the cross-section. Molds can be adjusted in several ways. In cases where the molds have not yet been created, 3D printing can create a small-scale model that can be easily fine-tuned to find the appropriate cross-section before creating the mold at full scale. However, existing molds can be slightly adjusted to change the thickness of various sections within a cross-section, which is more cost-effective than creating an entirely new mold. Typical extrusion molds for producing WPVC composites consist of a large outer mold, which controls the overall size of the WPVC hollow element, and small inner molds that block the material to create hollow sections during the extrusion process. Additionally, the inner molds have slightly larger holes than the size of the bolts, which are used to lock their position. The larger holes than the bolts allow for slight repositioning. The slight repositioning of inner molds can be made by loosening the bolts and adjusting the position of the inner mold slightly up, down, left, or right to achieve the preferred thickness. However, if the inner mold cannot be repositioned, new inner molds can be designed and created to replace the old one to increase or decrease the thickness in various parts without creating an entirely new mold. Before adjusting the thickness of each section, it is necessary to specify which parts should be adjusted to enhance flexural performance. Therefore, this research also aims to identify appropriate cross-section adjustments.

To identify the appropriate cross-section adjustments, parametric studies focus on the impact of variations in thickness on flexural performance. This can be achieved by adjusting the thickness within the WPVC composite hollow element while maintaining the same cross-sectional area and overall dimensions. This approach maintains production costs and facilitates the comparison of its effects on flexural performance. This research provides a prototype or guidance for glulam assembly with various cross-sectional shapes of WPVC composite, reducing the number of repetitive four-point bending tests needed to assess flexural performance.

EXPERIMENTAL

In the glulam method, GWPVC hollow members were assembled by bonding WPVC composite hollow elements with adhesive. The properties of the WPVC composite under tensile and compressive forces were tested to determine the stress–strain curve. Subsequently, these results were used to predict and simulate flexural performance under four-point bending conditions using AMIT and FEM, respectively. AMIT used MATLAB code based on Euler's beam theory, while FEM employed ABAQUS for modeling and simulation. The results obtained from AMIT and FEM were validated by experimental results to determine the most suitable method for use in the parametric study.

Materials for GWPVC Hollow Member

The GWPVC hollow member was assembled using WPVC composite hollow elements. The WPVC composite material consisted of 1:1 wood sawdust to PVC (by weight) and additives. Thermal stabilizers are used in PVC compounds such as Pb–Ba-based organic polyfluorene and polyfluorene. External and internal lubricants, such as a high molecular weight complex compatible lubricant and calcium stearate, are included. Additionally, emulsion PVC and processing aids are added to achieve the appropriate flow in the production process. The production process, as used previously (Pulngern *et al.* 2011, 2013, 2014; Eakintumas *et al.* 2022b), begins by drying wood particles at 80 °C for 24 h, blending them with PVC using a high-speed mixer, melting and blending them in a twin-screw extruder at 180 °C, and finally extruding them through a mold and solidifying using a cooling system. Two cross-sectional shapes are bonded with cyanoacrylate adhesive YOKOMO 505 from Taiwan during the assembly of the GWPVC hollow member.

Material Properties of WPVC Composite

The WPVC composite was tested under tensile and compressive forces following ASTM D638 (2014) and ASTM D6108 (2019), respectively. Specimens for tensile testing had dimensions of 19 mm × 165 mm × 2.8 mm, with a central width of 13 mm, as shown in Fig. 1(a), and the hollow specimens for compressive testing had dimensions of 19.6 mm × 22.63 mm × 39.2 mm, as shown in Fig. 1(b).

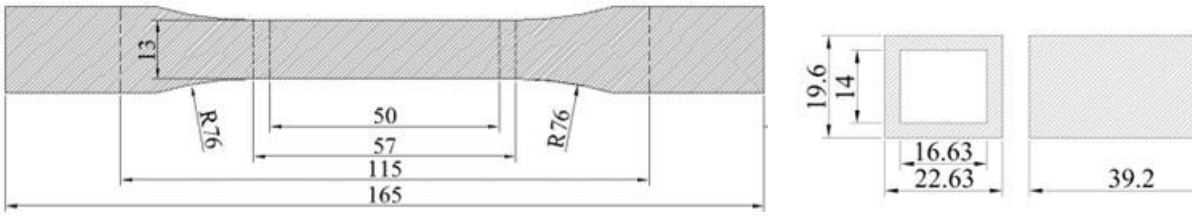

Fig. 1. Specimens for material properties testing in mm (a) Tensile test and (b) Compressive test

Strain gauges, 1 and 2 per specimen for tensile and compressive tests, respectively, were installed. Each test was performed on five specimens, and the results fit a curve. The constants *a* and *b* obtained from fitting the curve to the material properties under tensile or compressive force are determined for the Boxlucas1 function, as shown in Eq. 1,

$$\sigma = a(1 - e^{-b\varepsilon}) \quad (1)$$

where σ and ε represent stress and strain, respectively.

Bonding Test

The shear strength of the adhesive for bonding WPVC composite hollow elements to assemble the GWPVC hollow member was tested following ASTM D905 (2021). Specimens, sized 50.8 × 44.4 mm, were sanded with #120 or #80 grit sandpapers. After sanding, the prepared surfaces were cleaned with acetone. A cyanoacrylate adhesive was applied, and another WPVC composite piece was attached immediately without pressure. The adhesive was left to dry for a day at room temperature. Five specimens were prepared for each coarseness of sandpaper.

Preparing Specimens and Setting up the Test for Four-Point Bending

The GWPVC hollow member was assembled from WPVC composite hollow elements (PL-08A and DE-04) using the glulam method to create a double I-shape, as shown in Fig. 2(a). This assembly method followed the same preparation process as the bonding test specimens. Three specimens were prepared with a 2,130-mm span length (*L*) and a slenderness ratio of 15 (Sombatsompop *et al.* 2010). External loads were applied at *L*/3 and 2*L*/3 with a 10 mm/min loading rate following ASTM D198 (2022), and the deflection at mid-span was measured using two displacement transducers (DT), as shown in Fig. 2(b).

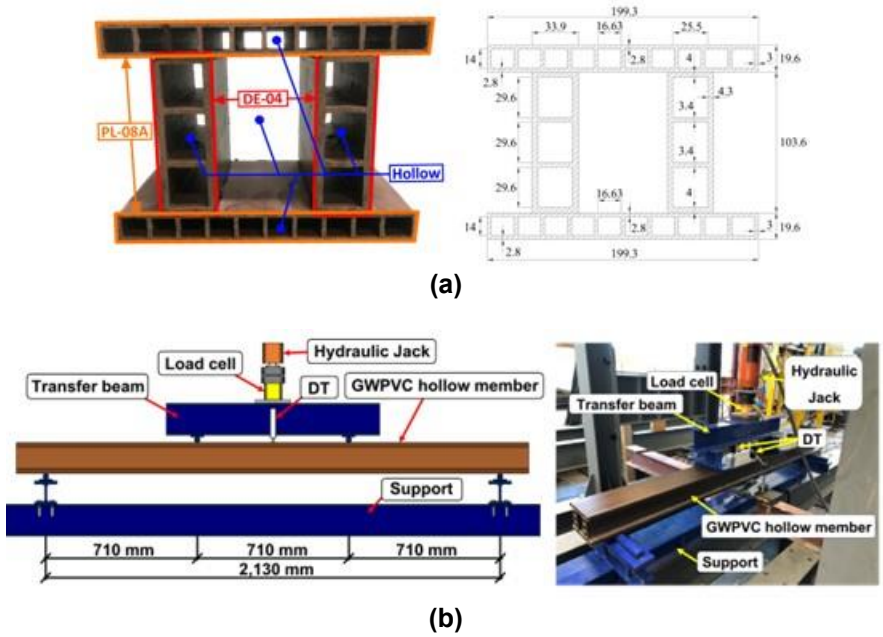

Fig. 2. The glulam WPVC composite hollow member specimen and testing setup (a) Cross-section of glulam WPVC composite hollow member (all values are given in mm) and (b) Flexural testing setup for glulam WPVC composite hollow member with a span length of 2,130 mm

Flexural Performance Prediction with AMIT

The AMIT predictions integrate a theoretical analysis of the GWPVC hollow member based on Euler's beam theory (Naghipour *et al.* 2011) with calculations using the iterative technique. The objective is to predict the flexural performance under four-point bending testing, assuming that it includes no delamination, small deflections, minimal shear deformation, and excludes buckling effects. The analysis assumes that the GWPVC hollow member is bent, resulting in a non-zero strain at the top. The equilibrium of the forces on the cross-section is employed to locate the neutral axis (NA) corresponding to that strain. Finally, Euler's beam theory is used to calculate the deflection and applied loads. The AMIT process is divided into two parts: locating the NA and determining GWPVC hollow member load–deflection curve**,** as shown in Fig. 3.

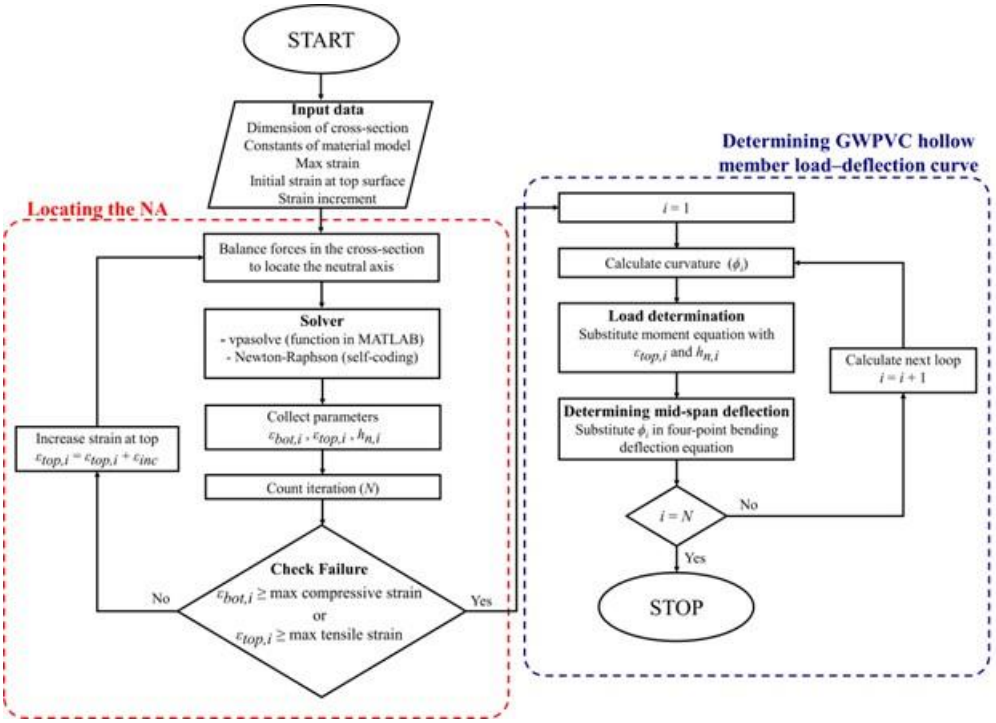

Fig. 3. Flowchart of the analytical method with iteration technique (AMIT) process for calculating load and deflection of glulam WPVC composite hollow member

Locating the neutral axis

It is assumed that the GWPVC hollow member is bent with a non-zero strain at the top and a linear strain distribution in the cross-section. The strain at each level can be expressed in terms of the strain at the top surface, as defined in Eq. 2

$$\varepsilon_y = \frac{\varepsilon_{top}}{h_n} \cdot y \quad (2)$$

where ε_{top}, h_n, y, and ε_y represent the strain at the top surface, the distance from the top surface to the NA, the distance from the NA to the strain location, and the strain at any level from the NA, respectively. The force (F) within the considered area is determined by substituting Eq. 2 into Eq. 3.

$$F = \int a(1 - e^{-b\varepsilon_y})\, dA \quad (3)$$

Subsequently, the location of the NA (h_n) is determined by solving the equilibrium of forces on the cross-section and substituting the non-zero strain value (the balancing method). Additionally, the strain values at the top and bottom surfaces of the GWPVC hollow member are calculated to monitor potential failure. These processes are repeated until the top or bottom strain exceeds the maximum strain obtained from material properties testing. The iterative process is facilitated using MATLAB software, and the details of each step are as follows:

1. The initial strain is defined at the top surface ($\varepsilon_{top,i}$), assuming the GWPVC hollow member is bent, as shown in Fig. 4(a).
2. The location of the NA ($h_{n,i}$) is calculated for each $\varepsilon_{top,i}$ using the equilibrium equations when the NA is aligned with the central web area, as shown in Fig. 4(b), expressed as Eq. 4.
3. Substituting Eq. 2 and Eq. 3 into Eq. 4 yields Eq. 5. Subsequently, Eq. 5 is solved using the Newton–Raphson method and the function to solve symbolic equations numerically (vpasolve) in MATLAB. Both methods are applied within a limited range for the location of the NA to determine the value of $h_{n,i}$. The results from both methods are cross-checked to ensure accuracy.

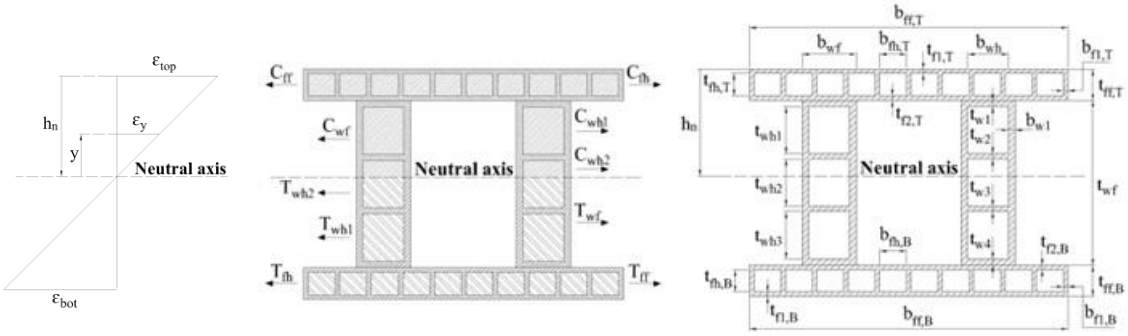

Fig. 4. GWPVC hollow member overview (a) strain distribution (b) force diagram and (c) cross-section

$$C_{ff} - C_{fh} + C_{wf} - C_{wh1} - C_{wh2} = T_{ff} - T_{fh} + T_{wf} - T_{wh1} - T_{wh2} \quad (4)$$

In Eq. 2, terms are as follows:

C_{ff} : Compressive force on the upper flange, excluding the cavities.

C_{fh} : Compressive force resulting from the cross-sectional area of the cavities in the upper flange.

C_{wf} : Compressive force on the web above the NA location, excluding the cavities.

C_{wh1}: Compressive force resulting from the area of the first cavities in the web above the NA location.

C_{wh2}: Compressive force resulting from the area of the second cavities in the web above the NA location.

T_{ff} : Tensile force on the lower flange, excluding the cavities.

T_{fh} : Tensile force resulting from the area of the cavities in the lower flange.

T_{wf} : Tensile force on the web below the NA location, excluding the cavities.

T_{wh1}: Tensile force resulting from the area of the first cavities in the web below the NA location.

T_{wh2}: Tensile force resulting from the area of the second cavities in the web below the NA location.

$$\int_{h_{n,i}-t_{ff}}^{h_{n,i}} a\left(1-e^{-b(\frac{\varepsilon_{top,i}}{h_{n,i}}\cdot y)}\right)b_{ff}dy \; -10\int_{h_{n,i}-t_{fl}-t_{fh}}^{h_{n,i}-t_{fl}} a\left(1-e^{-b(\frac{\varepsilon_{top,i}}{h_{n,i}}\cdot y)}\right)b_{fh}dy$$
$$+2\int_{0}^{h_{n,i}-t_{ff}} a\left(1-e^{-b(\frac{\varepsilon_{top,i}}{h_{n,i}}\cdot y)}\right)b_{wf}dy \; -2\int_{h_{n,i}-t_{ff}-t_{w1}-t_{wh}}^{h_{n,i}-t_{ff}-t_{w1}} a\left(1-e^{-b(\frac{\varepsilon_{top,i}}{h_{n,i}}\cdot y)}\right)b_{wh}dy$$
$$-2\int_{0}^{h_{n,i}-t_{ff}-2t_{w1}-t_{wh}} a\left(1-e^{-b(\frac{\varepsilon_{top,i}}{h_{n,i}}\cdot y)}\right)b_{wh}dy \; -\int_{H-h_{n,i}-t_{ff}}^{H-h_{n,i}} c\left(1-e^{-d(\frac{\varepsilon_{top,i}}{h_{n,i}}\cdot y)}\right)b_{ff}dy$$
$$+10\int_{H-h_{n,i}-t_{fl}-t_{fh}}^{H-h_{n,i}-t_{fl}} c\left(1-e^{-d(\frac{\varepsilon_{top,i}}{h_{n,i}}\cdot y)}\right)b_{fh}dy \; -2\int_{0}^{H-h_{n,i}-t_{ff}} c\left(1-e^{-d(\frac{\varepsilon_{top,i}}{h_{n,i}}\cdot y)}\right)b_{wf}dy$$
$$+2\int_{H-h_{n,i}-t_{ff}-t_{w1}-t_{wh}}^{H-h_{n,i}-t_{ff}-t_{w1}} c\left(1-e^{-d(\frac{\varepsilon_{top,i}}{h_{n,i}}\cdot y)}\right)b_{wh}dy$$
$$+2\int_{0}^{H-h_{n,i}-t_{ff}-2t_{w1}-t_{wh}} c\left(1-e^{-d(\frac{\varepsilon_{top,i}}{h_{n,i}}\cdot y)}\right)b_{wh}dy = 0 \qquad (5)$$

where *a* and *b* represent the constants obtained from the curves fit to the material properties under tensile force, while *c* and *d* represent the constants obtained from the curves fit to the material properties under compressive force.

4. The maximum strain at the bottom surface ($\varepsilon_{bot,i}$) is calculated in each iteration using the triangle proportionality theorem, as shown in Fig. 4(a).
5. The $\varepsilon_{top,i}$, $\varepsilon_{bot,i}$, and $h_{n,i}$ are recorded. The conditions are checked to determine whether to stop or proceed to the next iteration. The NA location calculation stops if $\varepsilon_{top,i}$ or $\varepsilon_{bot,i}$ exceeds the maximum strain from tensile or compressive testing. Otherwise, $\varepsilon_{top,i}$ is increased for the next iteration. Additionally, the number of iterations (N) for calculating the NA location is recorded for use as the iteration limit of the load and deflection calculations.

Determining GWPVC hollow member load–deflection curve

The load determination begins with calculating the moment capacity of the cross-section, which is obtained by summing the moments generated by all forces acting on the cross-section around the NA. Subsequently, the moment capacity is substituted into the bending moment equation for four-point bending to calculate the load. Calculating the deflection starts by determining the curvature using Eq. 6. The curvature is calculated based on the strain at the top surface and the NA location is referenced from the top surface. Furthermore, the analysis assumes a small deflection and employs a differential equation derived from Euler's beam theory, which approximates the curvature based on a ratio of the moment at its location and bending stiffness, as shown in Eq. 7.

$$\phi = \frac{\varepsilon(y)}{y} \qquad (6)$$

$$\phi \approx \frac{d^2\Delta(x)}{dx^2} = \frac{M(x)}{EI} \qquad (7)$$

where ϕ, $M(x)$, and EI represent the curvature, the moment at the location of x on the GWPVC hollow member, and the bending stiffness of the GWPVC hollow member, respectively.

The deflection (Δ) is determined from the curvature approximation in Eq. 7 by substituting the curvature into the four-point bending deflection equation, as presented in Eq. 8. The load and deflection calculations are facilitated using MATLAB for the iterative process. The details of each step are as follows:

$$\Delta(x=\frac{L}{2}) = \frac{M(x=\frac{L}{2})}{EI} \cdot \frac{(3L^2 - 4a^2)}{24} = \phi \cdot \frac{(3L^2 - 4a^2)}{24} \quad (8)$$

where L and a represent the span length and the loading span, respectively.

Load determination

The moment capacity (M_i) is calculated using Eq. 9 by substituting $\varepsilon_{top,i}$, $h_{n,i}$, and the dimensions of the cross-section, as illustrated in Fig. 4(c). Eq. 9 is specifically used to determine the moment capacity for $h_{n,i}$ aligned with the central cavity of DE-04.

$$\begin{aligned}
M_i = &\int_{h_n-t_{ff}}^{h_n} a\left(1 - e^{-b\left(\frac{\varepsilon_{top,i}}{h_{n,i}}\cdot y\right)}\right) b_{ff} y dy - 10\int_{h_n-t_{f1}-t_{fh}}^{h_n-t_{f1}} a\left(1 - e^{-b\left(\frac{\varepsilon_{top,i}}{h_{n,i}}\cdot y\right)}\right) b_{fh} y dy \\
&+ 2\int_{0}^{h_n-t_{ff}} a\left(1 - e^{-b\left(\frac{\varepsilon_{top,i}}{h_{n,i}}\cdot y\right)}\right) b_{wf} y dy - 2\int_{h_n-t_{ff}-t_{w1}-t_{wh}}^{h_n-t_{ff}-t_{w1}} a\left(1 - e^{-b\left(\frac{\varepsilon_{top,i}}{h_{n,i}}\cdot y\right)}\right) b_{wh} y dy \\
&- 2\int_{0}^{h_n-t_{ff}-2t_{w1}-t_{wh}} a\left(1 - e^{-b\left(\frac{\varepsilon_{top,i}}{h_{n,i}}\cdot y\right)}\right) b_{wh} y dy + \int_{H-h_n-t_{ff}}^{H-h_n} c\left(1 - e^{-d\left(\frac{\varepsilon_{top,i}}{h_{n,i}}\cdot y\right)}\right) b_{ff} y dy \\
&- 10\int_{H-h_n-t_{f1}-t_{fh}}^{H-h_n-t_{f1}} c\left(1 - e^{-d\left(\frac{\varepsilon_{top,i}}{h_{n,i}}\cdot y\right)}\right) b_{fh} y dy + 2\int_{0}^{H-h_n-t_{ff}} c\left(1 - e^{-d\left(\frac{\varepsilon_{top,i}}{h_{n,i}}\cdot y\right)}\right) b_{wf} y dy \\
&- 2\int_{H-h_n-t_{ff}-t_{w1}-t_{wh}}^{H-h_n-t_{ff}-t_{w1}} c\left(1 - e^{-d\left(\frac{\varepsilon_{top,i}}{h_{n,i}}\cdot y\right)}\right) b_{wh} y dy \\
&- 2\int_{0}^{H-h_n-t_{ff}-2t_{w1}-t_{wh}} c\left(1 - e^{-d\left(\frac{\varepsilon_{top,i}}{h_{n,i}}\cdot y\right)}\right) b_{wh} y dy
\end{aligned}$$

$$\begin{aligned}
M_i = &\frac{a h_{n,i}^{\,2}}{A_i^{\,2}}[b_{ff}\{(A_i+1)e^{-A_i}\} + (2b_{wf}-b_{ff})\{(B_i+1)e^{-B_i}\} - 10b_{fh}\{(C_i+1)e^{-C_i} \\
&- (D_i+1)e^{-D_i}\} - 2b_{wh}\{(E_i+1)e^{-E_i} - (F_i+1)e^{-F_i} + (G_i+1)e^{-G_i}\}] \\
&+ \frac{c h_{n,i}^{\,2}}{A_i^{\,2}}[b_{ff}\{(A'_i+1)e^{-A'_i}\} + (2b_{wf}-b_{ff})\{(B'_i+1)e^{-B'_i}\} - 10b_{fh}\{(C'_i+1)e^{-C'_i} \\
&- (D'_i+1)e^{-D'_i}\} - 2b_{wh}\{(E'_i+1)e^{-E'_i} - (F'_i+1)e^{-F'_i} + (G'_i+1)e^{-G'_i}\}] \quad (9)
\end{aligned}$$

where $A_i = b\varepsilon_{top,i}$, $B_i = \frac{b\varepsilon_{top,i}}{h_{n,i}}(h_{n,i}-t_{ff})$, $C_i = \frac{b\varepsilon_{top,i}}{h_{n,i}}(h_{n,i}-t_{f1})$, $D_i = \frac{b\varepsilon_{top,i}}{h_{n,i}}(h_{n,i}-t_{f1}-t_{fh})$,

$E_i = \frac{b\varepsilon_{top,i}}{h_{n,i}}(h_{n,i}-t_{ff}-t_{w1})$, $F_i = \frac{b\varepsilon_{top,i}}{h_{n,i}}(h_{n,i}-t_{ff}-t_{w1}-t_{wh})$, $G_i = \frac{b\varepsilon_{top,i}}{h_{n,i}}(h_{n,i}-t_{ff}-2t_{w1}-t_{wh})$,

$A'_i = \frac{d\varepsilon_{top,i}}{h_{n,i}}(H-h_{n,i})$, $B'_i = \frac{d\varepsilon_{top,i}}{h_{n,i}}(H-h_{n,i}-t_{ff})$, $C'_i = \frac{d\varepsilon_{top,i}}{h_{n,i}}(H-h_{n,i}-t_{f1})$, $D'_i = \frac{d\varepsilon_{top,i}}{h_{n,i}}(H-h_{n,i}-t_{f1}-t_{fh})$,

$E'_i = \frac{d\varepsilon_{top,i}}{h_{n,i}}(H\text{-}h_{n,i}\text{-}t_{ff}\text{-}t_{w1})$, $F'_i = \frac{d\varepsilon_{top,i}}{h_{n,i}}(H\text{-}h_{n,i}\text{-}t_{ff}\text{-}t_{w1}\text{-}t_{wh})$, and $G'_i = \frac{d\varepsilon_{top,i}}{h_{n,i}}(H\text{-}h_{n,i}\text{-}t_{ff}\text{-}2t_{w1}\text{-}t_{wh})$

The load is calculated by substituting M_i and a into the bending moment equation for four-point bending ($M_i = P_i \times a$). The moment of inertia (I_i) is determined for each iteration. The maximum stress of the GWPVC hollow member is calculated for each iteration. The number of loops for the calculated load is checked. If it is not equal N, the calculation proceeds to the next step. Otherwise, the calculation is stopped.

Determining mid-span deflection

The curvature (ϕ_i) for each iteration was calculated using Eq. 6 by substituting $\varepsilon_{top,i}$ and $h_{n,i}$. The deflection ($\Delta_i(x)$) is calculated by substituting ϕ_i into Eq. 8. The calculation of ϕ_i and $\Delta_i(x)$ is repeated N times.

After obtaining the load–deflection curve, the result is validated by comparing it with the experimental data. Furthermore, the AMIT result is compared with the FEM result to select the most suitable method for use in parametric studies.

Flexural Performance Simulated with FEM

The flexural performance of the GWPVC hollow member was simulated using FEM in ABAQUS. The model uses two cross-sections of WPVC composite hollow elements to form a double I-shape, which is connected with tie constraints to simulate adhesive bonding without slippage or separation (Eakintumas *et al.* 2022b). A simply supported configuration with a span length of 2,130 mm is used for four-point bending conditions. The material properties of the WPVC composite are assumed to be isotropic (Eakintumas *et al.* 2022b) to reduce complexity and make modeling more accessible. A hyper-elastic material, specifically the Marlow model, is chosen to simplify the material properties and represent isotropic properties with nonlinear characteristics (Pulngern *et al.* 2013). When selecting material properties, the tensile strength is approximately 1.5 times lower than the compressive strength (Pulngern *et al.* 2013). Therefore, the tensile property is chosen as the material model because its lower value will control the failure and provide a safety margin for application in other cross-sectional simulations.

Before using the material properties, the uniaxial tensile test results on five specimens are averaged by fitting the curve to the Boxlucas1 function in OriginLab. The outcome is used to evaluate the Marlow strain energy function, providing material properties for simulating the GWPVC hollow member. Additionally, a Poisson's ratio of 0.4 is applied (Eakintumas *et al.* 2022b). The element type of twenty-node quadratic brick elements with reduced integration (C3D20R) is employed, resulting in excellent performance under bending conditions and minimizing hourglassing despite the reduced number of integration points (Boumezbeur *et al.* 2023). The surfaces between the specimen and supports are modeled with normal behavior and hard contacts. The specimen surfaces are assigned as the slave surface, while the support surfaces are considered the master surface. This configuration prevents the specimen from penetrating the supports (Dassault Systèmes 2014). The tangential behavior is assumed to be frictionless, allowing the specimen to slide freely on the support after loads are applied at $L/3$ and $2L/3$ (710 and 1,420 mm). The simulation terminates if the maximum stress reaches the tensile strength or the maximum strain reaches the limit from tensile testing. After the simulation, the FEM result is validated with experimental data and compared to the AMIT results to determine which method is suitable for parametric studies.

Parametric Studies

After validating the AMIT and FEM results with experimental data, the most suitable method is chosen to investigate the impact of variations in the slenderness ratio and cross-section on the flexural performance of the GWPVC hollow member. The investigation begins with variations in span lengths, leading to changes in the slenderness ratio. Subsequently, variations in the flange and web thicknesses of DE-04 and PL-08A are considered while the overall size and total cross-sectional area are maintained.

RESULTS AND DISCUSSION

Material Properties for Tensile and Compressive Testing

The tensile and compressive properties of the WPVC composite were determined following ASTM D638 (2014) and D6108 (2019), respectively. Figure 5 shows the results for the tensile and compressive behavior of the WPVC composite.

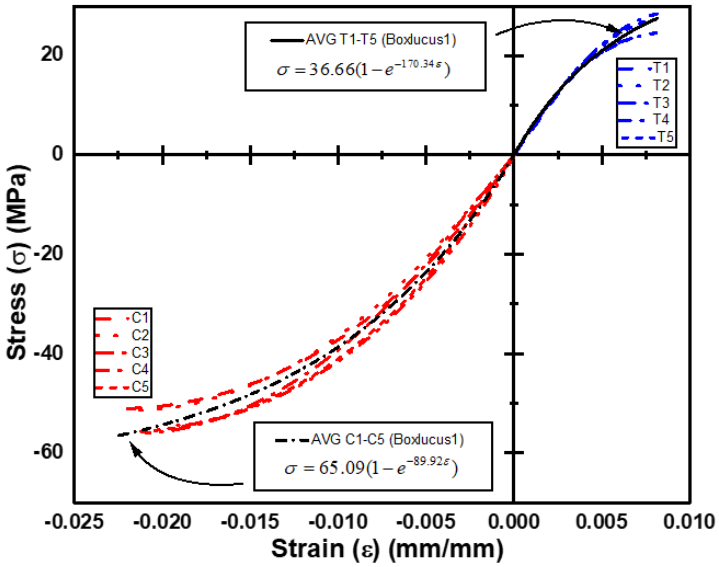

Fig. 5. Material properties testing and curves fit to the Boxlucus1 equation (CX denotes the behavior under compressive testing of WPVC composite specimen X, and TY represents the behavior of WPVC composite specimen Y under tensile testing)

Table 1. Material Model Constants for WPVC Composite and the Ultimate Stress and Strain under Tensile and Compressive Loading

	Tensile Test		Compressive Test	
Constants	***a***	***b***	***c***	***d***
	36.66	170.34	65.09	89.92
Ultimate stress (MPa) (%CV)	25.41 (8.82)		53.68 (4.33)	
Ultimate strain (μ) (%CV)	7,526 (9.31)		21,190 (5.65)	
R-Squared	0.99414		0.99178	

Curve-fitting was applied to average the results from tensile and compressive testing and determine the constants of the Boxlucas1 equation. The R-squared values for tensile and compressive testing were 0.99414 and 0.99178, respectively. The ultimate stress, ultimate strain, and constants of tensile and compressive testing for Eq. 1 are shown in Table 1.

Bonding Test Results

The bonding tests were conducted according to ASTM D905 (2021); the results are presented in Table 2. The control specimens exhibited a bonding strength of 7.93 MPa, with delamination observed at the bonded area, as shown in Fig. 6(a). Although the bonding strength of specimens sanded with #80 and #120 grit sandpapers could not be precisely calculated, it was estimated to exceed 7.93 MPa. This estimation was supported by the failures observed within the WPVC composite material (Figs. 6(b) and 6(c)), where all specimens failed due to the insufficient shear strength of the WPVC composite, and no debonding or slipping occurred in the bonded area. The bonding method with surface preparation using #80 and #120 grit sandpaper demonstrated perfect bonding and could withstand shear stress more effectively than the control specimens. These bonding strengths exceeded the requirements of the JAS234 (2003), which specifies a bond strength of 5.4 MPa for structural glued laminated timber (Nadir *et al.* 2016). A comparison between the control and prepared surfaces suggested that a rougher surface achieved better bonding. Thus, #80 and #120 grit sandpapers were chosen for surface preparation. Although #80 and #120 grit sandpaper are the same price, the #80 grit sandpaper takes less time to prepare the surface than the #120 grit. Thus, #80 grit sandpaper was selected to prepare the surfaces of WPVC composite hollow elements for assembling the GWPVC hollow member. Furthermore, bonding failure is assumed to occur at a strength limit of 7.93 MPa.

Table 2. Results of Testing the Bonding Strength Capability of Adhesives with Varying Surface Roughness Preparations in the Bonding Area

Specimen	Sandpaper Grit	Average Bonding Area (mm^2) (%CV)	Average Maximum Force (kN) (%CV)
Control	-	2,366.79 (0.43)	18.79 (8.16)
C-S120	#120	2,373.29 (0.45)	21.89 (5.16)
C-S80	#80	2,372.09 (0.99)	21.46 (6.25)

Note: C-SX refers to specimens assembled using cyanoacrylate adhesive and prepared surface with #X grit sandpapers.

(a) **(b)** **(c)**

Fig. 6. Failure of specimens for bonding test (a) Specimen without sanding (b) Specimen with sanding #120 grit sandpapers and (c) Specimen with sanding #80 grit sandpapers

Four-Point Bending Experiment

The four-point bending tests of GWPVC hollow members were conducted according to ASTM D198 (2022), and the results are shown in Fig. 7. The initial modulus of elasticity (MOE) was 5,140 MPa, and the MOR was 29.8 MPa for the NA locations assumed to align with the middle of the cross-section (the approximate method). The MOR was compared with previous research on WPVC composite hollow elements using the same mixture and production process and showed a 6.55% higher value for the flatwise loading direction and a 3.16% lower value for the edgewise loading direction (Pulngern *et al.* 2011). Additionally, compared with another study testing the four-point bending of WPVC composite hollow elements under similar conditions, the MOR was 19.3% lower for the flatwise loading direction and 1.55% higher for the edgewise loading direction (Pulngern *et al.* 2013). The differences in MOR may be attributed to variations in cross-sectional shape, area, and testing conditions that affect stress distribution within the specimens. For the maximum load and deflection of the GWPVC hollow member, the average values were 17.39 kN (CV 0.23%) and 47.76 mm (CV 0.51%), respectively.

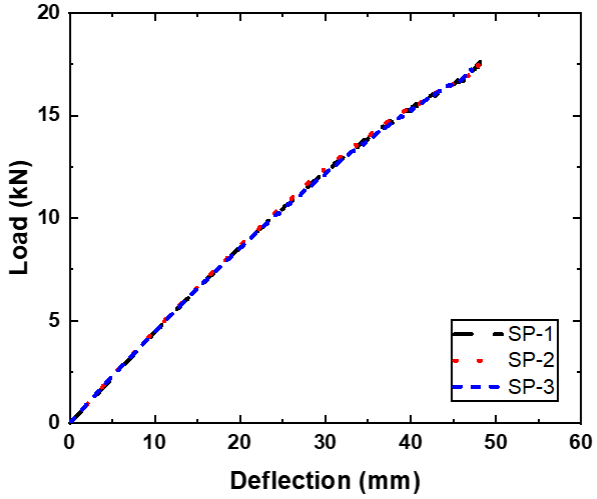

Fig. 7. Flexural testing of WPVC composite with four-point bending test (SP-X indicates the test results for specimen X in the laboratory)

All of the GWPVC hollow members exhibited flexural tensile failure in a brittle mode due to the lower tensile strength of the WPVC composite compared to its compressive strength. Furthermore, the failures occurred within the 710 to 1,420 mm range, as shown in Fig. 8, where these locations experienced the maximum bending moment while the shear force equals zero. Thus, the failure patterns were consistent with the locations of failures. When the bonded areas were examined, the specimens showed no delamination or separation, confirming the effectiveness of the bonding method for assembling GWPVC hollow members. The experimental results demonstrated similar load–deflection curves with minor differences, as shown in Fig. 7, showing that the glulam method can be applied to WPVC composite hollow elements, effectively controlling quality with very low variation in flexural behavior compared to glulam timber beams.

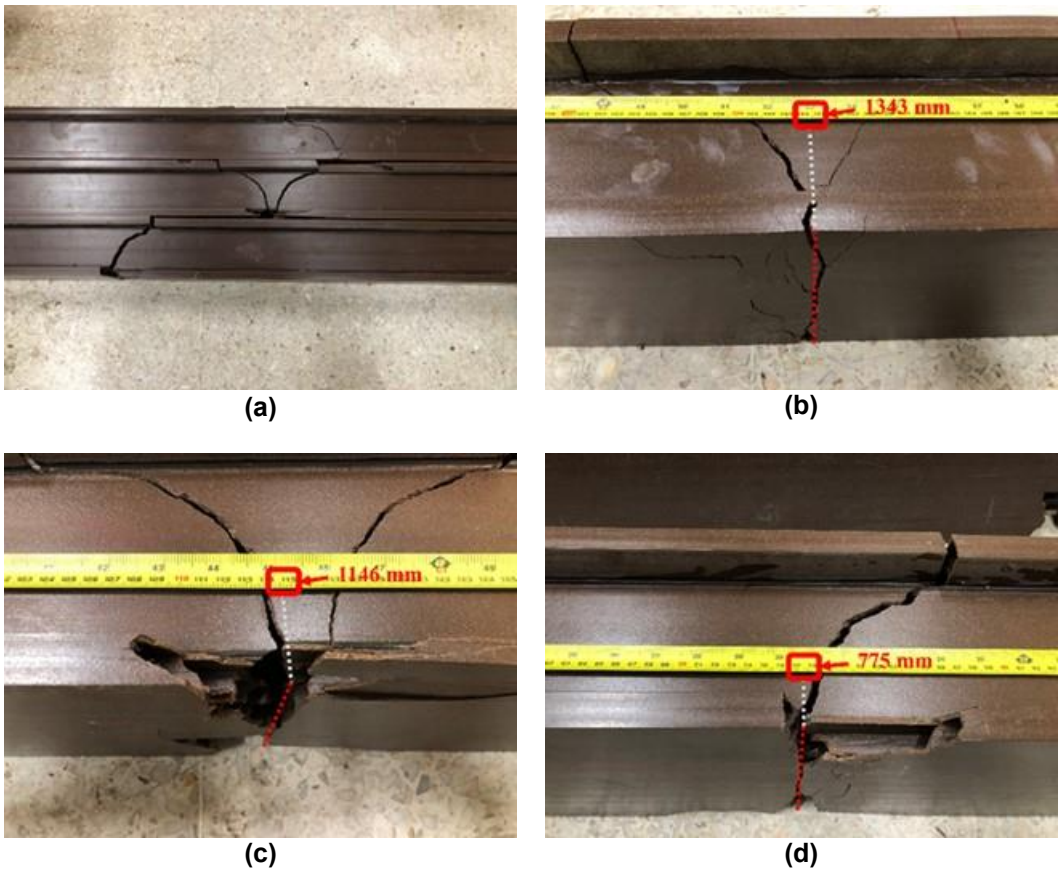

Fig. 8. Glulam WPVC composite hollow member failure: (a) Specimen failures (b) First specimen failure location (c) Second specimen failure location and (d) Third specimen failure location

Prediction with AMIT and Simulation with FEM

Validation of AMIT with experimental results

The AMIT predictions of the flexural performance of the GWPVC hollow member under four-point bending (balancing and approximate methods) are shown in Fig. 9.

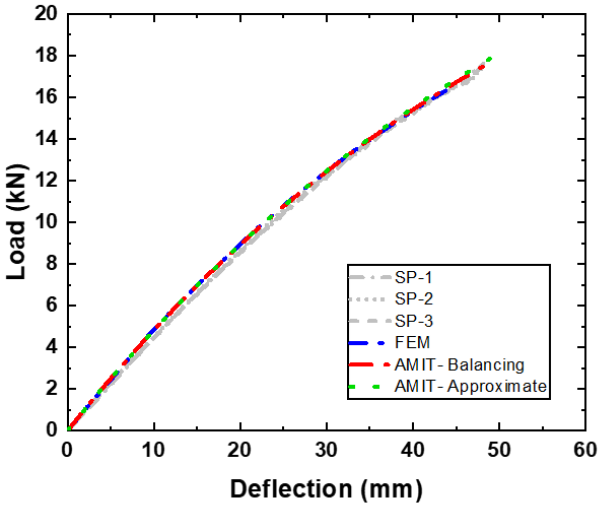

Fig. 9. Comparison of AMIT predictions, FEM simulation, and experimental results (SP-X indicates the test results for specimen X in the laboratory)

AMIT with the balancing method agreed with experimental results and provided a better outcome than the approximate method. The initial MOE from the balancing method was 5,450 MPa, differing by 6.14% from the experimental result. The differences in the initial MOE may arise from the material model obtained by averaging from multiple specimens. Moreover, imperfect shapes from the production process also affected the differences in the initial MOE. The imperfections were found in specific web and flange sections of GWPVC hollow members, with curved shapes in PL-08A, as shown in Fig. 10(a), and air bubbles detected in the DE-04, as shown in Fig. 10(b).

Fig. 10. Defect shapes of WPVC composite hollow elements (a) Web defect (curved shape) in PL-08A and (b) Air bubble in DE-04

The NA shifted toward the compression zone when the load or strain at the top increased, as shown in Fig. 11. The simplified Eq. 10 can also be used to find the NA accurately at any load level for four-point bending conditions and a slenderness ratio of 15. Furthermore, Eq. 11 can be applied to accurately determine the NA when the strain at the top of the GWPVC hollow member is known. This equation can be used not only for a simply supported condition but also for beams supported in other configurations, such as cantilever or overhanging, for any load type and level.

$$h_n = 72.934 - 0.204P - (1.452\times10^{-3})P^2 - (2.333\times10^{-4})P^3 \quad (10)$$

$$h_n = 72.922 - (6.666\times10^{-4})\varepsilon_{top} - (1.670\times10^{-8})\varepsilon_{top}^2 \quad (11)$$

where P is the load level in kN, ε_{top} is the strain at the top of the GWPVC hollow member in microstrain, and h_n is the distance between the NA and the top surface of the GWPVC hollow member in millimeters calculated from the balancing method.

The difference in the NA at the ultimate load of the GWPVC hollow member from AMIT with the approximate and balancing methods ranged from 5.84% to 6.44%. The NA obtained from Eq. 10 was used to recalculate the MOR more accurately, resulting in an average MOR value of 31.28 MPa, as indicated in Table 3. The ultimate load and maximum deflection predicted by AMIT with the balancing method were 17.54 kN and 48.37 mm, respectively. These values exceeded the experimental results by 0.86% and 1.28%, respectively. Meanwhile, using AMIT with the approximate method for predicting flexural performance resulted in an ultimate load and maximum deflection of 18.33 kN and 50.92 mm, respectively, higher than the experimental result by 5.41% and 6.62%, respectively. The failure of the GWPVC hollow member in the predictions made using both methods occurred in the tension zone, where the strain at the bottom reached the maximum tensile strain before the maximum compressive strain occurred at the top

surface. This failure pattern corresponded to the experimental results, where the failure was initiated in the tension zone.

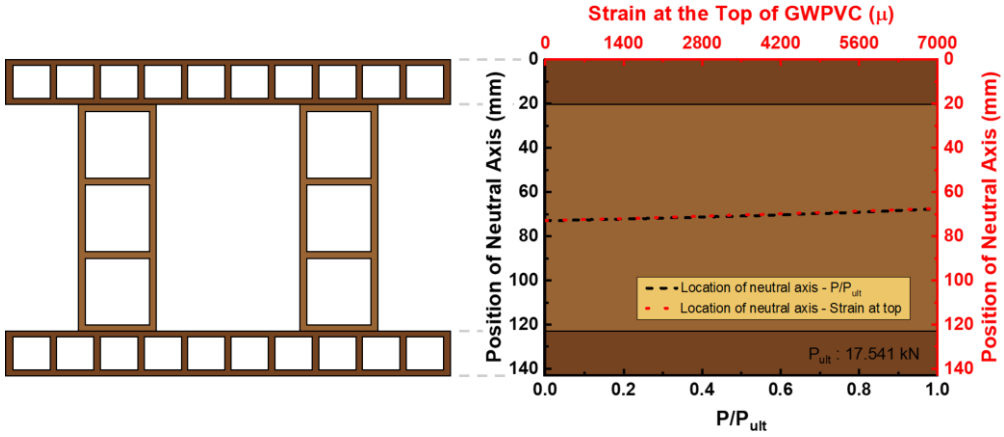

Fig. 11. Neutral axis (NA) location of GWPVC hollow member

Table 3. Comparison of Results Obtained from AMIT Predictions

Specimen codes	Ultimate Load (kN)			Location of NA at Break Point (mm)				MOR (MPa)			
	Exp	AMIT		Exp		AMIT		Exp		AMIT	
		Approx NA	Anlst NA	Approx NA	Formula	Approx NA	Anlst NA	Approx NA	Formula	Approx NA	Anlst NA
SP-1	17.60	18.33	17.54	71.40	67.62	71.40	67.64	30.11	31.54	31.37	31.42
SP-2	17.40			71.40	67.72			29.77	31.14		
SP-3	17.18			71.40	67.82			29.39	30.72		
AVG	17.39	18.33	17.54	71.40	67.72	71.40	67.64	29.76	31.13	31.37	31.42
CV	0.23	-	-	-	0.10	-	-	0.36	0.41	-	-

Note: Exp represents experimental results, Approx NA denotes the approximate NA location, which is aligned with the middle of the cross-section, Anlst NA indicates the NA location obtained from the balancing method at the breakpoint, Formula refers to the result of using Eq. 10 (the balancing method) to calculate the NA location for each ultimate load based on experimental data, SP refers to the experimental specimen, and CV represents coefficient of variation (%)

Validation of FEM with experimental results

In simulating the flexural performance of the GWPVC hollow member under four-point bending conditions using ABAQUS, the model was created with a length of 2,130 mm with 5- to 7.5-mm element sizes, as shown in Fig. 12(a). The simulation revealed an MOE of 5,410 MPa, which deviated from the experimental result by 5.18%. The ultimate load and maximum deflection were 16.4 kN and 44.1 mm, differing from the experimental results by 5.76% and 7.68%, respectively. The difference in the initial MOE of the simulation compared to the experimental results may be related to the assumed material properties. It was assumed to be an isotropic material, and a material model was assigned with a tensile property. The tensile property had an initial MOE 1.10% lower than the compressive property, resulting in a minor deviation of the initial MOE from the experimental results. The tensile property had a maximum stress 47.34% lower than the compressive property, decreasing the ultimate load of the simulation. Additionally, the deviation in simulation results may be caused by the neglect of imperfections in shape and air bubbles, which may reduce efficiency. This slight deviation in the simulation results

suggests that the material model assumptions and modeling methods for the GWPVC hollow member can be employed. Moreover, the failures observed in the simulation, which occurred in the tension zone, as shown in Fig. 12(b), correspond with the experimental failure (Fig. 8).

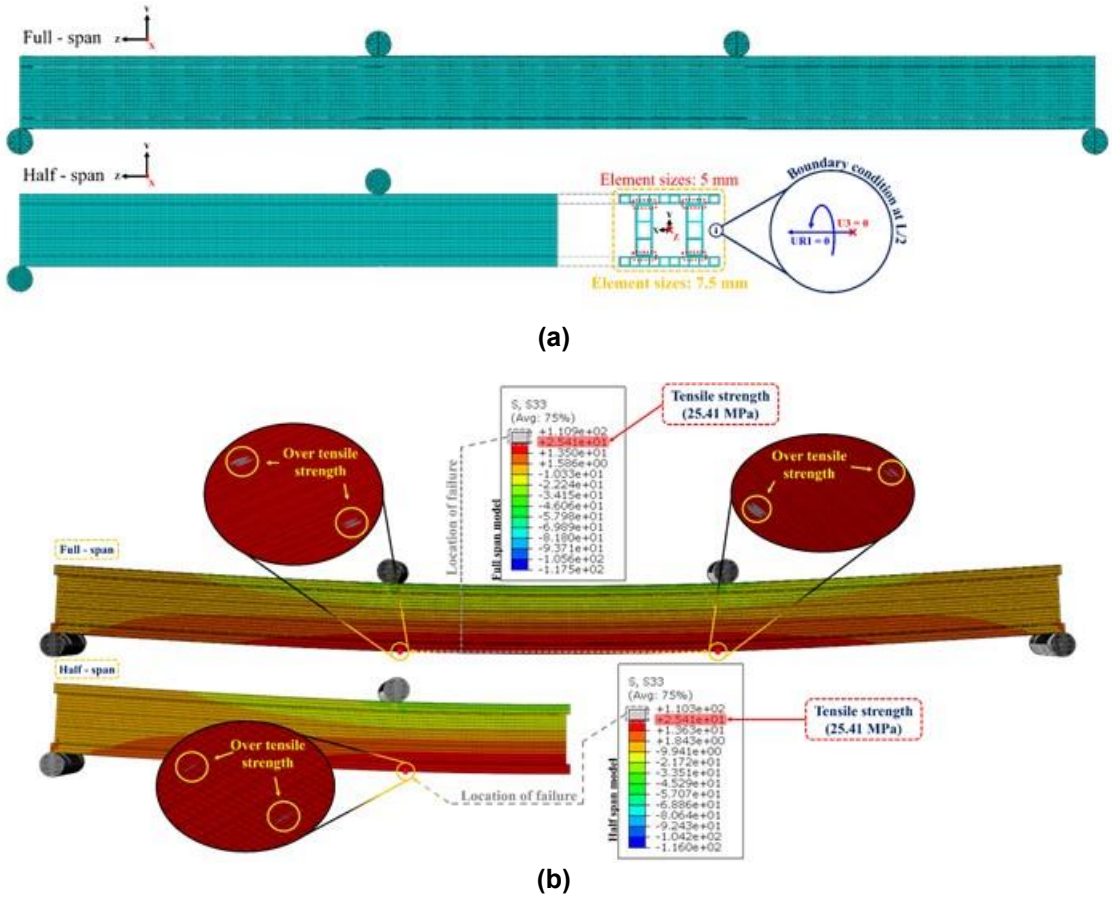

Fig. 12. Simulation with FEM of the GWPVC hollow member in half- and full-span configurations (a) Finite element model of the GWPVC hollow member in half- and full-span configurations and (b) The failure location of the GWPVC hollow member in half- and full-span configurations

Although the result of the simulation with the full-span model was close to the experimental results, it was highly computationally time-consuming. Therefore, the specimen was next modeled as a half-span instead of a full-span to reduce the time required (Garcia *et al.* 2016). The boundary conditions of the half-span model were assigned at *L*/2 by restricting the lengthwise movement and rotation perpendicular to the applied load, as shown in Fig. 12(a). The load–deflection curve from the half-span model was similar to that of the full-span model but required less time to complete. Therefore, the FEM simulation suggests using the half-span model with element sizes ranging from 5 to 7.5 mm.

When FEM and AMIT were compared, the material model in the FEM assigned only the tensile property, as mentioned above, while AMIT assigned both tensile and compressive properties. Therefore, the initial MOE and ultimate load from the FEM were slightly lower than those predicted by AMIT. Despite its slightly lower accuracy compared to AMIT, due to the material model being simplified to reduce the complexity in the modeling process, this FEM model can simulate the flexural performance of the GWPVC

hollow member with only a slight deviation from the experimental results. Additionally, FEM offers many advantages, such as lower material property requirements and the use of ABAQUS, which is readily available, making it a practical and efficient choice. FEM successfully simulated the flexural performance with minimal deviation and offers practical advantages due to its lower material property requirements and the availability of ABAQUS.

Parametric Studies

The results of AMIT and FEM were compared to determine the most suitable method for studying the flexural performance of GWPVC hollow members with varied span lengths and cross-sections. After validating the results from both AMIT and FEM through four-point bending tests, both methods agreed with the experimental results. Therefore, additional factors must be considered to decide the most suitable method.

AMIT is more suitable than FEM for several reasons, as shown in Table 4. First, it offers time efficiency, completing predictions in 1 to 6 h compared to FEM, which took over 10 h. AMIT allows for flexible strain increments and pauses during prediction, while FEM efficiency depends on adjusting the element size, with limitations. Second, AMIT shows simplicity, which is rooted in fundamental knowledge such as Euler's beam theory and coding without prior experience. Additionally, AMIT has lower associated licensing fees. Furthermore, AMIT's capability to handle a broader range of material properties, both tensile and compressive characteristics, enhances its accuracy. While general FEM can model with more complexity compared to AMIT, it also requires more experience to achieve high-accuracy results. However, both methods offer distinct advantages. Due to the facilitated accessibility without prior experience and its time efficiency, AMIT is the preferred choice for parametric studies.

Varying the slenderness ratio of the GWPVC hollow member under four-point bending conditions revealed that an increased span length resulted in a higher maximum deflection and decreased initial stiffness and ultimate load, as illustrated in Fig. 13. The ultimate load and maximum deflection can be calculated for any slenderness ratio using Eq. 12 and Eq. 13, respectively. However, these equations are considered for flexural failures of specimens when the slenderness ratio is 15 or higher (span length ≥ 2,130 mm). If the slenderness ratio is less than 15, then it is necessary to examine the failure due to shearing stress within the WPVC composite and the bonding area. Furthermore, when considering the GWPVC hollow member as a simply supported beam, it is necessary to ensure that the deflection limit does not exceed $L/300$, as specified in EN1995 (2004) for timber structures.

$$P_{ult} = \frac{261742.63}{(L/D)} \quad (12)$$

$$\delta_{ult} = 0.22(L/D)^2 \quad (13)$$

In Eqs. 12 and 13, P_{ult}, δ_{ult}, and L/D represent the ultimate load in N, maximum strain in mm, and the slenderness ratio, respectively.

Table 4. Comparison of AMIT and FEM

Aspect	Analytical Method with Iteration Technique (AMIT)	Finite Elements Method (FEM) (Simplified Material Model)
Time Required	1–6 hrs (Requires less time)	>8 hrs (Requires more time)
Visualisation	Code without any graphical	3D Model
Complexity	Low	Moderate
Basic knowledge	Based on Euler's beam and coding	Based on methodology for program usage
Consideration of Bulking and Shear Failure	Neglect	Considered
Condition Adjustment for Failure	Easier	Harder
Accuracy, as shown in Fig. 9 (in this research)	Highly accurate, aligns with experiment results	Highly accurate, aligns with experiment results
Database Usage	Tensile and compressive testing	Tensile testing
Testing Cost	USD 100 (Strain gauges for tensile test) USD 200 (Strain gauges for compressive test)	USD 100 (strain gauges for tensile test)
Licensing Cost (per year)	Low (MATLAB)	High (ABAQUS)
Software Program	MATLAB	ABAQUS

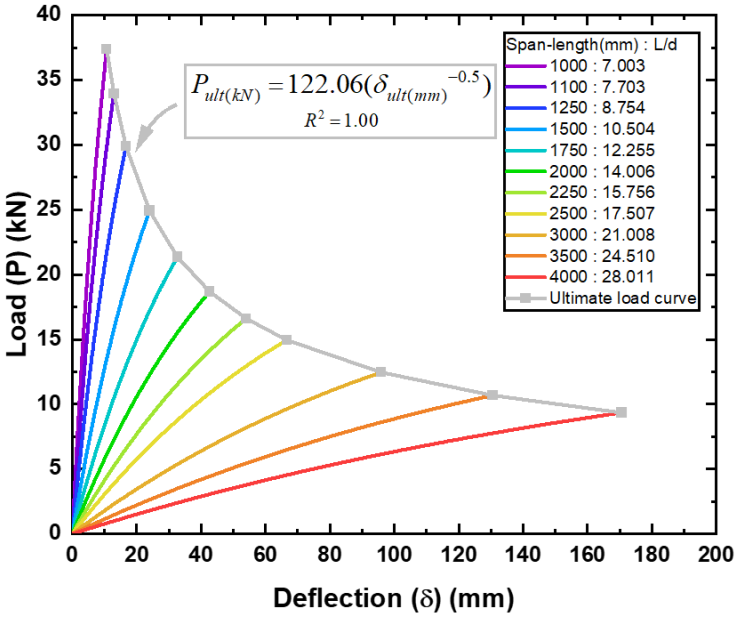

Fig. 13. Load–deflection curves for various span lengths of GWPVC hollow member

AMIT, employing the balancing method, was used to predict the impact of thickness variation in the flange and web or changes in the number of cavities in PL-08A with constant overall size and total area. The study assessed the effects on flexural performance, focusing on initial stiffness and ultimate load. Similar modifications were applied to the flange and web thickness of DE-04. The detailed results are as follows:

The variations in the cross-sectional thickness of PL-08A for each type slightly impacted flexural performance, as shown in Table 5. A comparison in types 1 and 2 with the control revealed that the outer flange ($t_{f1,T\&B}$) had a better impact on flexural performance than the inner flange ($t_{f2,T\&B}$). Increasing the outer flange area while reducing the inner flange area improved flexural performance, while the reverse resulted in decreased flexural performance. A comparison of types 3 and 4 suggested that the number of cavities or the entire web area of PL-08A does not significantly affect flexural performance. Therefore, the web area was redistributed to improve flexural performance. However, types 5 and 6 demonstrated that reducing the cavities and increasing the outer flange area enhanced flexural performance. In contrast, in types 7 and 8, reducing the cavities and increasing the inner flange area decreased flexural performance. Furthermore, reducing the cavities to increase the web thickness ($b_{f1,T\&B}$) in types 9 and 10 showed no impact on flexural performance, confirming the initial assumption that the prediction did not consider buckling and shearing effects. According to the prediction results, adjusting PL-08A by reducing the inner flange thickness and cavities to increase the thickness of the outer flange can enhance the flexural performance of the GWPVC hollow member.

The DE-04 cross-sectional thickness modifications significantly impacted flexural performance, as indicated in Table 6. In types 11 and 12, all flanges (t_{w1}, t_{w2}, t_{w3}, t_{w4}) had a better influence than the entire web (b_{w1}). Furthermore, this study also examined the thickness of each flange, which had the most significant impact on enhanced flexural performance in terms of initial stiffness and ultimate load.

In types 13 and 14, which compared the entire web to the first flange (t_{w1}), it was observed that the entire web had a better impact on the ultimate load. Despite an increased moment of inertia and initial stiffness because of the enhanced first flange, over-reinforcement in the compression zone and a reduced tensile-loaded area led to a decreased ultimate load. In types 15 and 16, comparing the entire web to the second flange (t_{w2}) revealed a better impact on flexural performance than the second flange, resulting in a decreased ultimate load for the same reason as types 13 and 14. The short distance from the NA to the second flange also reduced the moment of inertia and initial stiffness. Types 17 and 18 revealed that the third flange (t_{w3}) had a better influence than the entire web due to an increased area under tensile load. Expanding the tension zone, which had lower properties than the compressive zone, resulted in an increased ultimate load. However, the moment of inertia and initial stiffness decreased for the same reasons as types 15 and 16. Finally, types 19 and 20 showed that the fourth flange (t_{w4}) had a significantly better impact than the entire web, resulting in a higher ultimate load for the same reason as types 17 and 18. The increased distance from the NA to the fourth flange, almost equal to that of types 13 and 14, resulted in a nearly equal increase in the moment of inertia and initial stiffness, comparable to types 13 and 14. In conclusion, modifying the thickness of DE-04 by redistributing the web area to the fourth flange can significantly enhance flexural performance.

Table 5. AMIT Results for Modified GWPVC Hollow Member with Adjusted PL-08A Thicknesses

Model	Modified	Number of Hollows	Thickness (mm)					Initial Moment of Inertia ($\times 10^3$ mm^4) (% Diff to control)	Initial Stiffness (kN·m^2) (% Diff to control)	Ultimate Load (kN) (% Diff to control)
			b_{fh}	t_{fh}	b_{f1}	t_{f1}	t_{f2}			
Control	-	10	16.67	14.00	3.00	2.80	2.80	14,814.69	80.81	17.54
Type 1	PL-08A	10	16.67	14.00	3.00	2.00	3.60	14,352.66 (-3.12)	78.44 (-2.94)	17.12 (-2.40)
Type 2		10	16.67	14.00	3.00	3.60	2.00	15,270.78 (+3.08)	83.23 (+2.99)	17.96 (+2.38)
Type 3		8	21.54	13.51	3.00	3.04	3.04	14,820.72 (+0.04)	80.90 (+0.11)	17.54 (+0.02)
Type 4		6	29.72	13.06	3.00	3.27	3.27	14,824.37 (+0.07)	80.92 (+0.13)	17.55 (+0.03)
Type 5		8	21.54	13.51	3.00	3.29	2.80	14,960.45 (+0.98)	81.62 (+1.00)	17.67 (+0.75)
Type 6		6	29.72	13.06	3.00	3.74	2.80	15,093.62 (+1.88)	82.30 (+1.85)	17.79 (+1.43)
Type 7		8	21.54	13.51	3.00	2.80	3.29	14,680.43 (-0.91)	80.12 (-0.86)	17.42 (-0.71)
Type 8		6	29.72	13.06	3.00	2.80	3.74	14,553.06 (-1.77)	79.46 (-1.67)	17.30 (-1.39)
Type 9		8	20.79	14.00	3.67	2.80	2.80	14,815.31 (0.00)	80.81 (0.00)	17.54 (0.00)
Type 10		6	27.72	14.00	4.71	2.80	2.80	14,814.48 (0.00)	80.81 (0.00)	17.54 (0.00)

The symbols are specified in Fig. 4(c).

Table 6. AMIT Results for GWPVC Hollow Members with Adjusted DE-04 Thicknesses

Model	Modified	Number of Hollows	Thickness (mm)									Initial Moment of Inertia ($\times 10^3$ mm^4) (% Diff to control)	Initial Bending Stiffness (kN·m^2) (% Diff to control)	Ultimate Load (kN) (% Diff to control)
			b_{w1}	b_{wh}	t_{w1}	t_{wh1}	t_{w2}	t_{wh2}	t_{w3}	t_{wh3}	t_{w4}			
Control	-	3	4.20	25.50	4.00	29.60	3.40	29.60	3.40	29.60	4.00	14,814.69	80.81	17.54
Type 11	DE-04	3	3.20	25.50	6.03	26.89	5.43	26.89	5.43	26.89	6.03	14,948.87 (+0.91)	81.61 (+0.99)	17.69 (+0.84)
Type 12			2.20	25.50	8.06	24.18	7.46	24.18	7.46	24.18	8.06	15,041.75 (+1.53)	82.12 (+1.62)	17.79 (+1.44)
Type 13			3.20	25.50	12.13	21.47	3.40	29.60	3.40	29.60	4.00	15,183.40 (+2.49)	82.69 (+2.33)	17.11 (-2.47)
Type 14			2.20	25.50	20.25	13.35	3.40	29.60	3.40	29.60	4.00	15,211.67 (+2.68)	82.67 (+2.29)	16.42 (-6.42)
Type 15			3.20	25.50	4.00	29.60	11.53	21.47	3.40	29.60	4.00	14,491.27 (-2.18)	78.97 (-2.28)	16.89 (-3.71)
Type 16			2.20	25.50	4.00	29.60	19.65	13.35	3.40	29.60	4.00	14,124.05 (-4.66)	76.92 (-4.81)	16.39 (-6.57)
Type 17			3.20	25.50	4.00	29.60	3.40	29.60	11.53	21.47	4.00	14,636.10 (-1.21)	79.93 (-1.09)	17.86 (+1.82)
Type 18			2.20	25.50	4.00	29.60	3.40	29.60	19.65	13.35	4.00	14,581.91 (-1.57)	79.93 (-1.09)	18.49 (+5.41)
Type 19			3.20	25.50	4.00	29.60	3.40	29.60	3.40	21.47	12.13	15,180.39 (+2.47)	82.99 (+2.70)	18.87 (+7.58)
Type 20			2.20	25.50	4.00	29.60	3.40	29.60	3.40	13.35	20.25	15,205.75 (+2.64)	83.14 (+2.89)	19.77 (+12.68)

The symbols are specified in Fig. 4(c).

Adjusting the mold thickness for PL-08A and DE-04 resulted in prediction of significant enhancement, as shown in Fig. 14. The adjustments for PL-08A included enhancing the outer flange, reducing the inner flange by 0.8 mm, and decreasing the number of cavities to 8 and 6 for types 21 and 22, respectively. The modifications to DE-04 included enhancing the fourth flange and reducing the entire web by 1 and 2 mm for types 21 and 22, respectively. The outcomes for types 21 and 22 demonstrated significant increases of 10.84% and 16.83% in ultimate load and a 6.52% and 7.58% increase in initial stiffness, respectively.

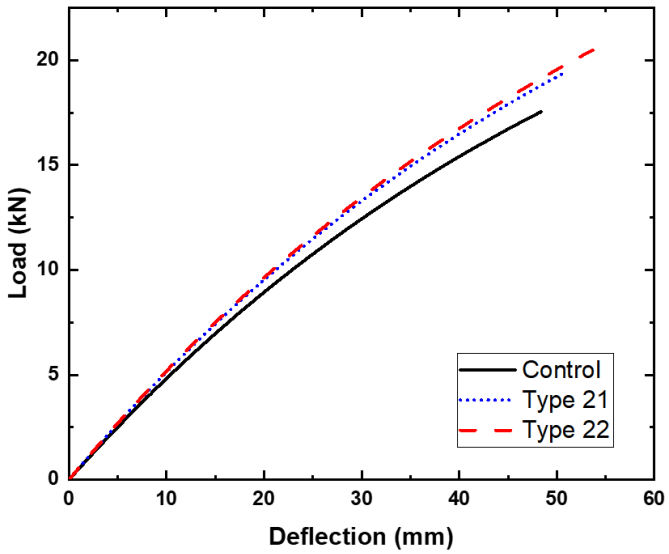

Fig. 14. Flexural performance of GWPVC hollow members before and after slight adjustments to the thicknesses of PL-08A and DE-04

CONCLUSIONS

1. The most suitable method for assembling the glulam wood poly(vinyl chloride) composite (GWPVC) hollow member includes preparing the surface of WPVC composite hollow elements through sanding with #80 grit sandpaper and applying cyanoacrylate adhesive without pressure.
2. The four-point bending tests on the GWPVC hollow member revealed an average ultimate load of 17.4 kN, an average maximum deflection of 47.8 mm, a modulus of elasticity (MOE) of 5,140 MPa, and a modulus of rupture (MOR) using the approximate and balancing methods at 29.8 and 31.1 MPa, respectively. The failures occurred with flexural tensile failure for all specimens within the L/3 to 2L/3 range, exhibiting a brittle failure mode without delamination along the length of each specimen.
3. For comparison, the predictions of the analytical method with iteration technique (AMIT) and finite element method (FEM) differed from the experimental results by 0.86% and 5.76% in ultimate load, 1.28% and 6.91% in maximum deflection, and 0.86% and 5.18% in initial MOE, respectively. The AMIT prediction and FEM simulation closely aligned with the experimental results, indicating that these methods can be used to assess WPVC composite flexural performance in glulam applications.

However, the bonding strength must be sufficient until the specimen fails.

4. When predicting the flexural performance with AMIT, the balancing method is more accurate than the approximate method. However, the approximate method is suitable for rough predictions less than 10% different from the experimental results. The balancing method calculates the MOR based on the theoretical neutral axis (NA) location, while the approximate method uses approximation, providing MOR estimates with less than a 5% difference from theoretical results.
5. Improved flexural performance in GWPVC hollow members through minor mold adjustments while maintaining the cross-sectional area is achieved by reducing the web and inner flange thicknesses while increasing the outer flange thickness for PL-08A. Similarly, for DE-04, the entire web thickness is decreased, and the thickness of the flange subjected to tension and farthest from the NA location will increase.

ACKNOWLEDGMENTS

This project is funded by National Research Council of Thailand (NRCT) and King Mongkut's University of Technology Thonburi (KMUTT). The authors gratefully acknowledge the financial support provided by the Petchra Pra Jom Klao Ph.D. Research Scholarship with Grant No. 18/2563, King Mongkut's University of Technology Thonburi. Special gratitude is extended to V.P. Wood Co., Ltd. for their generous provision of the WPVC composite materials.

REFERENCES CITED

ASTM D638 (2014). "Standard test method for tensile properties of plastics," ASTM International, West Conshohocken, PA.

ASTM D6108 (2019). "Standard test method for compressive properties of plastic lumber and shapes," ASTM International, West Conshohocken, PA.

ASTM D905 (2021). "Standard test method for strength properties of adhesive bonds in shear by compression loading," ASTM International, West Conshohocken, PA.

ASTM D198 (2022). "Standard test methods of static tests of lumber in structural sizes," ASTM International, West Conshohocken, PA.

Bedon, C., and Fragiacomo, M. (2015). "Numerical and analytical assessment of the buckling behaviour of Blockhaus log-walls under in-plane compression," *Engineering Structures* 82, 134-150. DOI: 10.1016/j.engstruct.2014.10.033

Bhaskar, J., Haq, S., and Yadaw, S. (2012). "Evaluation and testing of mechanical properties of wood plastic composite," *Journal of Thermoplastic Composite Materials* 25(4), 391-401. DOI: 10.1177/0892705711406158

Boumezbeur, K., Khebizi, M., and Guenfoud, M. (2023). "Finite element modeling of static and cyclic response of functionality graded material beams," *Asian Journal of Civil Engineering* 24, 579-591. DOI: 10.1007/s42107-022-00519-8

Chetanachan, W., Sookkho, D., Sutthitavil, W., Chantasatrasamy, N., and Sinsermsuksakul, R. (2001). "PVC wood: A new look in construction," *Journal of Vinyl and Additive Technology* 7(3), 134-137. DOI: 10.1002/vnl.10280

Chaochanchaikul, K., Rosarpitak, V., and Sombatsompop, N. (2013). "Photodegradation

profiles of PVC compound and wood/PVC composites under UV weathering," *eXPRESS Polymer Letters* 7(2), 146-160. DOI: 10.3144/expresspolymlett.2013.14

Chen, J., Teng, Z., and Wu, J. (2017). "Recycling of waste FRP and corn straw in wood plastic composite," *Polymer Composites* 38(10), 2140-2145. DOI: 10.1002/pc.23789

Dassault Systèmes (2014). "Contact formulations in Abaqus/Standard," in: *ABAQUS (2014) Analysis User's Manual, Version 6.14*, Dassault Systemes Simulia, Inc.

Eakintumas, W., Pulngern, T., Rosarpitak, V., and Sombatsompop, N. (2022a). "Experimental investigation of lateral resisting elements for the wood polyvinyl chloride composite log-house under in-plane lateral loads," *Journal of Vinyl and Additive Technology* 28(1), 153-171. DOI: 10.1002/vnl.21877

Eakintumas, W., Pulngern, T., Rosarpitak, V., and Sombatsompop, N. (2022b). "Load-bearing capacity of wood polyvinyl chloride composite log-walls with openings strengthened with steel flat bars via experimental and numerical studies," *Structures* 37, 242-254. DOI: 10.1016/j.istruc.2022.01.003

EN1995 (2004). "Eurocode 5: Design of timber structures - Part 1-1: General - Common rules and rules for buildings," British Standards, London.

Falk, R. H., and Colling, F. (1995). "Laminating effects in glued-laminated timber beams," *Journal of Structural Engineering* 121(12), 1857-1863. DOI: 10.1061/(ASCE)0733-9445(1995)121:12(1857)

Garcia, C., Lotz, T., Martinez, M., Artemev, A., Alderliesten, R., and Benedictus, R. (2016). "Fatigue crack growth in residual stress fields," *International Journal of Fatigue* 87, 326-338. DOI: 10.1016/j.ijfatigue.2016.02.020

Glišović, I., Stevanović, M., and Todorović, M. (2016). "Flexural reinforcement of glulam beams with CFRP plates," *Materials and Structures* 49, 2841-2855. DOI: 10.1617/s11527-015-0690-7

Hamid, N. H. A., Ahmad, M., Suratman, M. N., and Abu, F. (2015). "Bending strength of finger jointed kelat wood (Syzygium spp.) as affected by finger length and orientation," *Advanced Materials Research*, 1134, 138-142. DOI: 10.4028/www.scientific.et/AMR.1134.138

Issa, C., and Kmeid, Z. (2005). "Advanced wood engineering: glulam beams," *Construction and Building Materials* 19(2), 99-106. DOI: 10.1016/j.conbuildmat.2004.05.013

İşleyen, Ü. K., Ghoroubi, R., Mercimek, Ö., Anil, Ö., and Erdem, R. T. (2021). "Behavior of glulam timber beam strengthened with carbon fiber reinforced polymer strip for flexural loading," *Journal of Reinforced Plastics and Composites* 40(17-18), 665-685. DOI: 10.1177/0731684421997924

JAS234 (2003). "Japanese agricultural standard for structural glued laminated timber," Japanese Agricultural Standard, Tokyo.

Jeamtrakull, S., Kositchaiyong, A., Markpin, T., Rosarpitak, V., and Sombatsompop, N. (2012). "Effects of wood constituents and content, and glass fiber reinforcement on wear behavior of wood/PVC composites," *Composites Part B: Engineering* 43(7), 2721-2729. DOI: 10.1016/j.compositesb.2012.04.031

Jian, B., Mohrmann, S., Li, H., Li, Y., Ashraf, M., Zhou, J., and Zheng, X. (2022). "A review on flexural properties of wood-plastic composites," *Polymers* 14(19), article 3942. DOI: 10.3390/polym14193942

Kanking, K., Pulngern, T., Rosarpitak, V., and Sombatsompop, N. (2021). "Temperature profiles and electric energy consumption for wood/Poly(vinyl chloride) composite and fibre cement board houses," *Journal of Building Engineering* 42, article 102784.

DOI: 10.1016/j.jobe.2021.102784

Kanking, S., Pulngern, T., Rosarpitak, V., and Sombatsompop, N. (2023). "Mechanical performance and anti-fungal and anti-algal properties for teakwood/parawood/PVC composites in UV-weathering and seawater immersion conditions," *BioResources* 18(3), 5599-5622. DOI: 10.15376/biores.18.3.5599-5622

Khelifa, M., Celzard, A., Oudjene, M., and Ruelle, J. (2016). "Experimental and numerical analysis of CFRP-strengthened finger-jointed timber beams," *International Journal of Adhesion and Adhesives* 68, 283-297. DOI: 10.1016/j.ijadhadh.2016.04.007

Kositchaiyong, A., Rosarpitak, V., Hamada, H., and Sombatsompop, N. (2014). "Anti-fungal performance and mechanical-morphological properties of PVC and wood/PVC composites under UV-weathering aging and soil-burial exposure," *International Biodeterioration & Biodegradation* 91, 128-137. DOI: 10.1016/j.ibiod.2014.01.022

Luo, T., and Cheng, S. (2021). "The effect of recycled WPC on the performance of composite materials," *IOP Conference Series: Earth and Environmental Science* 692(3), article 032092. DOI: 10.1088/1755-1315/692/3/032092

Maricar, S., Sulendra, K., Listiawaty, H., and Baide, H. O. (2022). "The flexural strength of glue laminated timber beams based on deflection and strain rate with four point bending loading system," *IOP Conference Series: Materials Science and Engineering* 1212, article 012034. DOI: 10.1088/1757-899X/1212/1/012034

Mohamad, W. H. W., Razlan, M. A., and Ahmad, Z. (2011). "Bending strength properties of glued laminated timber from selected Malaysian hardwood timber," *International Journal of Civil & Environmental Engineering* 11(4), 7-12.

Mrówczyński, D., Gajewski, T., and Garbowski, T. (2021a). "Application of the generalized nonlinear constitutive law in 2D shear flexible beam structures," *Archives of Civil Engineering* 67(3), 157-176. DOI: 10.24425/ace.2021.138049

Mrówczyński, D., Gajewski, T., and Garbowski, T. (2021b). "The generalized constitutive law in nonlinear structural analysis of steel frames," in: *Modern Trends in Research on Steel, Aluminium and Composite Structures*, M. Gizejowski *et al.* (eds), pp. 120-126. DOI: 10.1201/9781003132134-12

Nadir, Y., and Nagarajan, P. (2014). "The behavior of horizontally glued laminated beams using rubber wood," *Construction and Building Materials* 55, 398-405. DOI: 10.1016/j.conbuildmat.2014.01.032

Nadir, Y., Nagarajan, P., Ameen, M., and M, M. A. (2016). "Flexural stiffness and strength enhancement of horizontally glued laminated wood beams with GFRP and CFRP composite sheets," *Construction and Building Materials* 112, 547-555. DOI: 10.1016/j.conbuildmat.2016.02.133

Naghipour, M., Nematzadeh, M., and Yahyazadeh, Q. (2011). "Analytical and experimental study on flexural performance of WPC-FRP beams," *Construction and Building Materials* 25(2), 829-837. DOI: 10.1016/j.conbuildmat.2010.06.104

Naghipour, M., Arefi, S. L., and Nematzadeh, M. (2013). "Performance of longitudinal grooves to prevent debonding of GFRP sheets used for the reinforcement of WPC beams," *Journal of Civil Engineering and Management* 20(2), 761-776. DOI: 10.1080/19648189.2013.815136

Pattamasattayasonthi, N., Chaochanchaikul, K., Rosarpitak, V., and Sombatsompop, N. (2011). "Effects of UV weathering and a CeO_2-based coating layer on the mechanical and structural changes of wood/PVC composites," *Journal of Vinyl and Additive Technology* 17(1), 9-16. DOI: 10.1002/vnl.20246

Peixoto, L. S., Soriano, J., Mascia, N. T., and Pellis, B. P. (2022). "Bending behavior of steel bars reinforced Glulam beams considering the homogenized cross section," *Wood Material Science & Engineering* 17(1), 533-539. DOI: 10.1080/17480272.2021.1900392

Prachayawarakorn, J., Khamsri, J., Chaochanchaikul, K., and Sombatsompop, N. (2005). "Effects of compatibilizer type and rubber-wood sawdust content on the mechanical, morphological, and thermal properties of PVC/LDPE blend," *Journal of Applied Polymer Science* 102(1), 598-606. DOI: 10.1002/app.24324

Prachayawarakorn, J., Khunsumled, S., Thongpin, C., Kositchaiyong, A., and Sombatsompop, N. (2008). "Effects of silane and MAPE coupling agents on the properties and interfacial adhesion of wood-filled PVC/LDPE blend," *Journal of Applied Polymer Science* 108(6), 3523-3530. DOI: 10.1002/app.27973

Pulngern, T., Padyenchean, C., Rosarpitak, V., Prapruit, W., and Sombatsompop, N. (2011). "Flexural and creep strengthening for wood/PVC composite members using flat bar strips," *Materials & Design* 32(6), 3431-3439. DOI: 10.1016/j.matdes.2011.02.005

Pulngern, T., Chimkhlai, A., Rosarpitak, V., and Sombatsompop, N. (2013). "Analytical, numerical and experimental investigations on flexural strengthening for wood/PVC composite members using flat bar strips," *Construction and Building Materials* 41, 545-556. DOI: 10.1016/j.conbuildmat.2012.12.017

Pulngern, T., Kaewkalya, P., Rosarpitak, V., and Sombatsompop, N. (2014). "Experimental and computational investigations of creep responses of wood/PVC composite members," *International Polymer Processing* 29(3), 307-316. DOI: 10.3139/217.2927

Pulngern, T., Eakintumas, W., Rosarpitak, V., and Sombatsompop, N. (2017). "Compressive load, thermal and acoustic properties of wood/polyvinyl chloride composite log-wall panels," *Journal of Reinforced Plastics and Composites* 36(16), 1183-1193. DOI: 10.1177/0731684417699712

Pulngern, T., Udtaranakron, T., and Chanto, K. (2020). "Physical and mechanical behaviors of thermally modified rubberwood glulam beam under sustained and cyclic loading," *Wood and Fiber Science* 52(3), 298-312. DOI: 10.22382/wfs-2020-028

Ratanawilai, T., and Taneerat, K. (2018). "Alternative polymeric matrices for wood-plastic composites: Effects on mechanical properties and resistance to natural weathering," *Construction and Building Materials* 172, 349-357. DOI: 10.1016/j.conbuildmat.2018.03.266

Roman, K., Szemán, B., Szabó, Z., and Szabó, K. (2018). "Mechanical properties and structural changes of PVC-wood composites," in: *MultiScience - XXXII. microCAD International Multidisciplinary Scientific Conference*, Miskolc, Magyarország. DOI: 10.26649/musci.2018.015

Shah, B., Matuana, L., and Heiden, P. (2005). "Novel coupling agents for PVC/wood-flour composites," *Journal of Vinyl and Additive Technology* 11(4), 160-165. DOI: 10.1002/vnl.20056

Sombatsompop, N., Chaochanchaikul, K., Phromchirasuk, C., and Thongsang, S. (2003). "Effect of wood sawdust content on rheological and structural changes, and thermo-mechanical properties of PVC/sawdust composites," *Polymer International* 52(12), 1847-1855. DOI: 10.1002/pi.1386

Sombatsompop, N., and Chaochanchaikul, K. (2004). "Effect of moisture content on mechanical properties, thermal and structural stability and extrudate texture of

poly(vinyl chloride)/wood sawdust composites," *Polymer International* 53, 1210-1218. DOI: 10.1002/pi.1535

Sombatsompop, N., and Chaochanchaikul, K. (2005). "Average mixing torque, tensile and impact properties, and thermal stability of poly(vinyl chloride)/sawdust composites with different silane coupling agents," *Journal of Applied Polymer Science* 96(1), 213-221. DOI: 10.1002/app.21422

Sombatsompop, N., Taptim, K., Chaochanchaikul, K., Thongpin, C., and Rosarpitak, V. (2008). "Improvement of structural and thermal stabilities of PVC and wood/PVC composite by Zn and Pb stearates, and zeolite," *Journal of Macromolecular Science, Part A: Pure and Applied Chemistry* 45(7), 534-541. DOI: 10.1080/10601320802100572

Sombatsompop, N., Prapruit, W., Chaochanchaikul, K., Pulngern, T., and Rosarpitak, V. (2010). "Effects of cross section design and testing conditions on the flexural properties of wood/PVC composite beams," *Journal of Vinyl and Additive Technology* 16(1), 33-41. DOI: 10.1002/vnl.20202

Staszak, N., Gajewski, T., and Garbowski, T. (2021). "Generalized nonlinear constitutive law applied to steel trapezoidal sheet plates," in: *Modern Trends in Research on Steel, Aluminium and Composite Structures*, Routledge, pp. 185-191. DOI: 10.1201/9781003132134-21

Staszak, N., Garbowski, T., and Ksit, B. (2022). "Application of the generalized nonlinear constitutive law in numerical analysis of hollow-core slabs," *Archives of Civil Engineering* 68(2), 124-145. DOI: 10.1201/9781003132134-21

Tunsakul, P. (2006). *Engineering Properties of Wood Plastic Composite (WPC) : Experimental Studies*, Master's Thesis, King Mongkut's University of Technology Thonburi, Bangkok, Thailand.

Udtaranakron, T., Pulngern, T., and Sombatsompop, N. (2023). "Analytical and experimental investigation of the flexural and bond adhesive properties of thermally modified rubberwood and hybrid glulam beams with WPVC composites," *Structures* 58, 105498. DOI: 10.1016/j.istruc.2023.105498

Ulaşan, H., Bajraktari, A., Döngel, N., Imirzi, H. Ö., and Söğütlü, C. (2023). "Modulus of elasticity and flexural behavior of glulam beams reinforced with steel mesh in different mesh openings," *Materials* 16(12), article 4307. DOI: 10.3390/ma16124307

Yang, X., and Zhang, W. (2021). "Finite element analysis of bending behavior of steel plate reinforced glulam beams," in: *Artificial Intelligence and Advanced Manufacture (AIAM2021)*, New York, pp. 2949-2955. DOI: 10.1145/3495018.3501212

Zamli, A. O. A., Hassan, R., Sidek, M. N. M., Awaludin, A., Anshari, B., Hamid, N. H. A., and Sapuan, S. M. (2022). "Flexural performance of strengthened glued laminated (GLULAM) timber beam using glass fibre-reinforced polymer (GFRP)," *Green Infrastructure* 75-92. DOI: 10.1007/978-981-16-6383-3_6

Article submitted: April 26, 2024; Peer review completed: May 25, 2024; Revised version received: June 9, 2024; Accepted: June 11, 2024; Published: June 18, 2024.
DOI: 10.15376/biores.19.3.5197-5226